A Wideband, Wide Scanning Tightly Coupled Dipole Array With Integrated Balun (TCDA-IB)

Jonathan P. Doane, *Member, IEEE*, Kubilay Sertel, *Senior Member, IEEE*, and John L. Volakis, *Fellow, IEEE*

***Abstract*—A key challenge in the design of wideband dipole phased arrays is the design of equally wideband baluns which are sufficiently compact to fit within the unit cell (typically $< \lambda/10$ in the linear dimension at low frequencies). In this paper, we exploit the reactance of a compact Marchand balun as an impedance matching network for each array element. The elimination of bulky external baluns results in a significant reduction of size, weight and cost, while the bandwidth is simultaneously improved by over 30%, compared to standard feeding techniques. In this manner, a tightly coupled dipole array with an integrated balun (TCDA-IB) is developed which achieves 7.35:1 bandwidth (0.68 – 5.0 GHz) while scanning to $\pm 45^\circ$ in all directions, subject to $\mathrm{VSWR} < 2.65:1$. In a dual-polarization configuration, the TCDA-IB has low cross polarization of < -20 dB over the majority of the band. Measured results are presented for a prototype 8×8 element TCDA-IB, showing good agreement with simulation.**

***Index Terms*—Antenna arrays, broadband antennas, impedance matching, phased arrays.**

I. Introduction

WIDE band antennas and arrays are essential for high-resolution radar and tracking systems, high data rate communication links, and multi-waveform, multi-function front-ends. Various array technologies have been developed that are capable of extremely wide bandwidth (up to 10:1 or more) [1]–[4]. However, many existing designs are limited by their electrical thickness, scanning performance, or use of lossy materials. Tightly coupled dipole arrays (TCDAs) are low profile and have wide bandwidth, good scan performance, and low cross polarization [5]–[7]. However, the TCDA feed must include baluns or 180° hybrids that can sustain similarly wide bandwidths. Ideally, a small balun could be integrated within each unit cell for a lightweight, low profile implementation. However the available volume is quite limited, particularly for arrays operating above 500 MHz. For example, a TCDA operating over a 6:1 bandwidth of 750–4500 MHz may have a 30 mm element-element spacing ($< \lambda/13$ at 750 MHz), with the ground plane spaced a similar distance below the dipoles. Integration of wideband baluns within this volume is quite difficult, and previous attempts have yielded bandwidths of 4:1 or less [8]–[13]. Commercially available passive baluns at microwave frequencies are generally either narrow-band or are large, heavy and expensive, and active balun circuits are limited to receive-only applications. Another technique is to avoid baluns altogether and use shorting posts to mitigate common mode resonances, resulting in 5:1 bandwidth after external impedance matching [14]. However, for maximum bandwidth and performance, TCDAs currently must use bulky external baluns or 180° hybrids located below the ground plane [15]. This significantly increases the total size, weight, and cost of the array.

A major challenge in developing practical passive broadband baluns is obtaining efficient, wideband operation in a small size. For example, a Marchand balun requires both very high- and very low-impedance transmission lines for maximum bandwidth [16]. These features are difficult to implement in a compact volume, resulting in an increase of reactive mismatch. Printed Marchand baluns have been used with dipoles [11]–[13], but yield reduced bandwidth versus differential feeds. Nevertheless, this limitation may be mitigated by tuning the reactance of the balun to cancel that of the array, as is often done in Vivaldi arrays [1]. That is, the balun may be viewed as part of the impedance matching network for the array. Here, we employ a similar reactive cancellation technique for TCDAs and demonstrate that the inclusion of a reactive balun can actually improve the overall bandwidth compared to a TCDA that is fed differentially. We refer to this design approach as the TCDA with integrated balun (TCDA-IB).

A preliminary version of the TCDA-IB concept was first reported in [17] and [18]. In this paper we provide full measured results of this preliminary design which demonstrates a wide operational bandwidth of 6.6:1 while scanning to 45° in the principal and intercardinal planes. Additionally, we present an updated version of the TCDA-IB which includes several improvements, as listed below:

- The bandwidth has been further optimized to 7.35:1, with $\mathrm{VSWR} \leq 2.65:1$ while scanning to 45° in all planes.
- The unit-cell spacing was increased from 87% to 93% of $\lambda_{high}/2$, resulting in reduced element count while still avoiding grating lobes across the entire scan volume.
- A dual-polarized implementation is provided, with low cross-polarization of < -20 dB over most of the band (-13 dB worst case), although the impedance bandwidth is reduced slightly to 6.9:1.

The improvement in performance was obtained by using an updated circuit model, based on a simple TCDA equivalent circuit from [5]. Here, we propose an adjustment to this model

Manuscript received October 27, 2012; revised February 13, 2013; accepted May 07, 2013. Date of publication June 07, 2013; date of current version August 30, 2013. This work was supported in part by NAVAIR under Contract No. N68936-09-C-0099.

The authors are with Ohio State University, ElectroScience Laboratory, Columbus, OH 43212 USA (e-mail: doane.15@osu.edu).

Color versions of one or more of the figures in this paper are available online at http://ieeexplore.ieee.org.

Digital Object Identifier 10.1109/TAP.2013.2267199

which accounts for the presence of vertical feed lines, and provides improved accuracy when scanning the array. By using this circuit along with full-wave simulations, optimization of the array over the entire scan volume can be performed quickly and efficiently.

The paper is organized as follows. Section II reviews the TCDA concept and the introduces the improved equivalent circuit. Section III discusses the integration of a Marchand balun within the TCDA unit cell, and demonstrates how it can be used to improve the array's impedance bandwidth. A technique for reducing the input impedance to 50 Ω without impedance transformers is also provided. Section IV presents the details of the physical implementation of the updated TCDA-IB design. Section V demonstrates how the TCDA-IB may be implemented as a dual-polarized array, exhibiting low cross-polarization. Section VI presents construction details and measured results for an 8×8 element implementation of the preliminary TCDA-IB design from [17]. Our overall conclusions are provided in Section VII.

II. Simple Equivalent Circuits for TCDAs

A TCDA uses horizontal dipoles placed above a conducting ground plane, as shown in Fig. 1. By capacitively coupling neighboring dipoles, the array supports currents at wavelengths which greatly exceed the dimension of a single element. Moreover, the dipole inductance and inter-element capacitance serve to cancel the reactance of the nearby ground plane over a wide bandwidth.

An approximate equivalent circuit for the TCDA was proposed in [5], and is shown in Fig. 2. In this circuit, the dipole inductance is represented by L_{dipole}, and the inter-element capacitance is denoted as $C_{coupling}$. The substrate, superstrate, and free space layers are represented by transmission line sections with properties determined by the propagating Floquet mode within each corresponding layer. The admittances of the fundamental TE and TM Floquet modes are given in [19]

$$Y_{00}^{TE} = \frac{k_{z00}}{\omega \mu_0 \mu_r} \tag{1}$$

$$Y_{00}^{TM} = \frac{\omega \epsilon_0 \epsilon_r}{k_{z00}}. \tag{2}$$

For both modes, the propagation constant in the $\hat{\mathbf{z}}$ direction is $k_{z00} = k_0\sqrt{\mu_r \epsilon_r}\cos\theta_r$, where k_0 is the free space wavenumber, ϵ_r and μ_r are the relative material properties of each layer (i.e., substrate, superstrate, free space). The scan angle θ is illustrated in Fig. 1, and the corresponding angle of refraction within each layer is given by $\theta_r = \sin^{-1}(\sin\theta/\sqrt{\mu_r\epsilon_r})$.

For linearly polarized arrays, the TE mode is excited when scanning in the H-plane ($\phi = 0°$) and the TM mode is excited when scanning in the E-plane ($\phi = 90°$). The impedance of each transmission line section in Fig. 2 when scanning in the E- and H-planes is given by [20]

$$Z_r^E = \frac{d_E}{d_H}\frac{1}{Y_{00}^{TM}} = \eta\sqrt{\frac{\mu_r}{\epsilon_r}}\frac{d_E}{d_H}\cos\theta_r \tag{3}$$

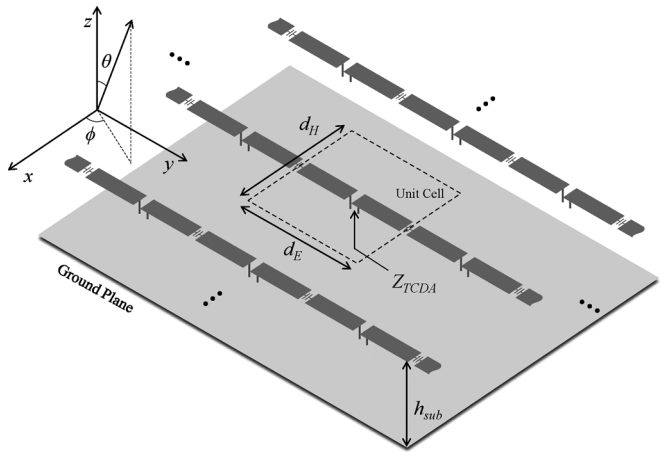

Fig. 1. A TCDA consisting of capacitively coupled dipole elements, placed above a conducting ground plane. The dipoles are aligned with the y-axis and the ground plane is normal to the z-axis. Substrate and superstrate materials (not shown) may also be included.

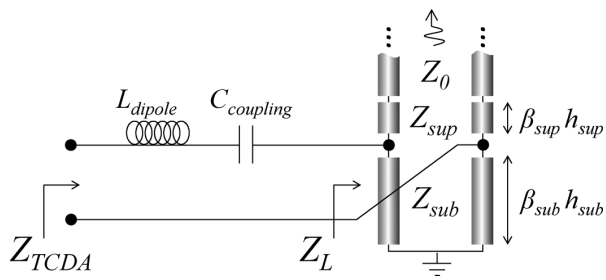

Fig. 2. Equivalent circuit for the TCDA proposed in [5], reproduced from [17]. Optimized circuit values at broadside are: $Z_0 = Z_{sub} = 188\ \Omega$, $Z_{sup} = 144\ \Omega$, $L_{dipole} = 3.0$ nH, $C_{coupling} = 2.0$ pF, $\beta_{sub}h_{sub} = 84°$, $\beta_{sup}h_{sup} = 64°$, with all electrical lengths given at 2.5 GHz.

$$Z_r^H = \frac{d_E}{d_H}\frac{1}{Y_{00}^{TE}} = \eta\sqrt{\frac{\mu_r}{\epsilon_r}}\frac{d_E}{d_H}\frac{1}{\cos\theta_r}. \tag{4}$$

The propagation constant for each line is given by

$$\beta_r = k_{z00} = k_0\sqrt{\mu_r\epsilon_r}\cos\theta_r. \tag{5}$$

Here, $\eta \approx 377\ \Omega$ is the characteristic impedance of free space, d_E is the E-plane (y-dimension) element spacing, and d_H is the H-plane (x-dimension) element spacing. Note that scanning in the intercardinal planes will excite both TE and TM modes simultaneously, which cannot be represented by the circuit of Fig. 2. However, the impedance bandwidth of a TCDA over a given conical scan volume is typically limited by the E- and H-plane responses, and thus the intercardinal response can usually be neglected for initial design optimization.

A. Validation of the TCDA Circuit Model

To evaluate the accuracy of the equivalent circuit, we considered a TCDA implementation as shown in Fig. 3, with dipoles that are printed on a vertically oriented printed circuit board. The dipole's inductance is controlled by the height h_{dipole}, and the inter-element capacitance is created by the overlap w_{cap} of the dipole arms that are printed on opposite sides of the PCB.

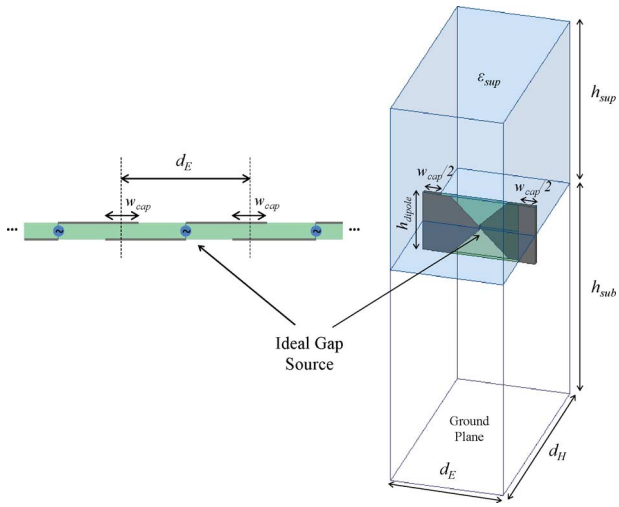

Fig. 3. Implementation of a TCDA unit cell, using vertical printed dipoles with arms on opposite sides of a thin PCB. The model does not include a realistic feed, rather the dipole is fed with an ideal 100 Ω gap source. On the left is a cross section of the PCB, showing the layout of the dipoles with overlapping arms.

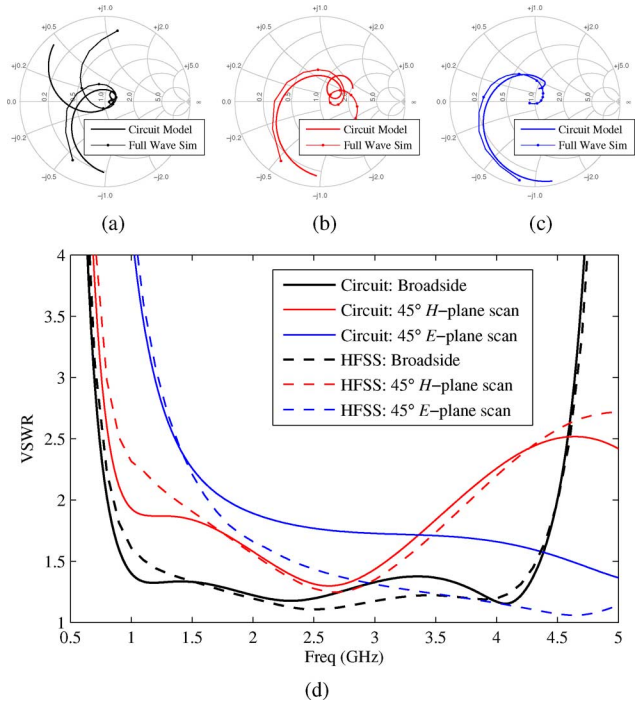

Fig. 4. Reflection coefficient of TCDA without feed, using the equivalent circuit model (Fig. 2) and the full wave simulation (Fig. 3). (a) Broadside scan. (b) 45° E–plane scan. (c) 45° H–plane scan. (d) VSWR of both models for each scan position. Other than h_{dipole}, all array dimensions are directly computed from the corresponding circuit values and have not been fine-tuned. (a) Broadside. (b) 45° H-plane scan. (c) 45° E-plane scan.

The spacing between the dipoles and the ground plane is h_{sub}, and the thickness of the dielectric superstrate is h_{sup}.

For reasons discussed in the following sections, we fix the impedance of the substrate and free space transmission lines at $Z_0 = 188\ \Omega$, corresponding to a rectangular unit cell with $d_E = 14$ mm and $d_H = 28$ mm. The impedance of the superstrate transmission line was set at $Z_{sup} = 144\ \Omega$, corresponding to a superstrate dielectric constant of $\epsilon_{sup} = 1.7$. The dipole was fed by a 100 Ω lumped gap source. Under these conditions, the remaining circuit parameters were optimized for maximum bandwidth using a genetic algorithm provided by AWR Microwave Office. Due to the simplicity of the circuit, optimization is relatively fast with convergence in less than one minute. The resulting optimized values are listed in the caption of Fig. 2, and the response is shown in Fig. 4.

With the exception of the dipole inductance, each physical dimension of the array can be directly computed from the corresponding circuit value, and the unit cell of Fig. 3 then simulated using Ansys HFSS v.14. The physical thicknesses of the substrate and superstrate are determined directly from the electrical length of the corresponding transmission lines, and $C_{coupling}$ is computed using a parallel plate capacitor model. The inductance L_{dipole} was then tuned by adjusting h_{dipole} until the simulation was roughly in agreement with the circuit model. Using a 0.25 mm thick board of Rogers 4350B, the optimal dipole dimensions are found to be $w_{cap} = 4.2$ mm and $h_{dipole} = 7.6$ mm.

The resulting response of the full-wave simulation is compared to the circuit model in Fig. 4 at broadside, and when scanning to 45° in the principle planes. Other than h_{dipole}, all dimensions of the array are computed directly from the optimized circuit model and have not been fine-tuned. It is clear that the circuit of Fig. 2 provides a good representation of the scanning TCDA. The model is of course not perfect, especially at higher frequencies where the simple inductance L_{dipole} is insufficient to account for the actual electrical length of the dipole. Improved accuracy could be obtained by using a more sophisticated analytical model such as [21]. Nevertheless, the circuit model of Fig. 2 yields a good initial design, and because of its simplicity provides a convenient reference for fine-tuning full-wave simulations.

However, both the above circuit and physical model are incomplete because neither accounts for the presence of the feed. As such, its accuracy is reduced when analyzing realistic TCDAs that include feed structures. We will show next how this limitation can be mitigated with a minor adjustment to the equivalent circuit.

B. Improved Equivalent Circuit for a TCDA With Feed

In a practical implementation, a TCDA must be excited by feed lines running from the ground plane to the dipoles. Thus, the above representation of the substrate as a homogeneous slab is insufficient. At broadside and when scanning in the H-plane, the feed lines do not have much effect, since the substrate mode is TE and the electric field polarization is normal to the vertical feed. However, when scanning in the E-plane, the presence of a feed has a significant impact on the substrate fields.

The effect of the feed can be seen in Fig. 5, where the electric field is plotted for two TCDAs, each scanned to 45° in the E-plane. Although the radiating dipoles are the same for both arrays, the first TCDA is fed by an ideal gap source, whereas the second TCDA contains a realistic feed structure. For the TCDA without feed lines, the substrate fields are accurately represented by the fundamental TM Floquet mode. However, when the feed

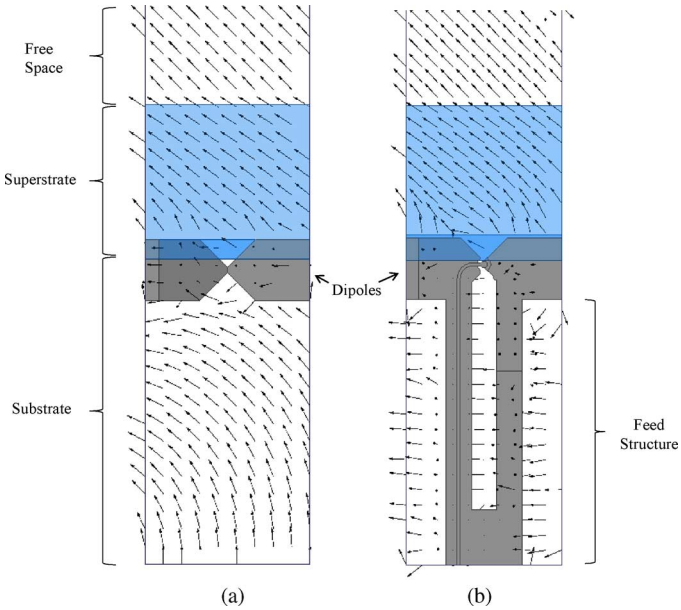

Fig. 5. Electric field in the unit cell of the TCDA, when scanning to 45° in the E-plane. (a) A TCDA unit cell with ideal gap source and no feed structure. In this case, the fields in the substrate, superstrate, and above the array are all well represented by the fundamental TM Floquet mode. (b) A TCDA unit cell with vertical conducting feed lines. The fields in the substrate are strongly influenced by the feed and form a guided quasi-TEM mode.

structure is introduced, the electric field in the substrate couples strongly to the feed lines, forming a guided quasi-TEM mode. Unlike the TM Floquet mode described by (3) and (5), the impedance and propagation constant of the TEM mode in the substrate do not significantly vary when scanning in the E-plane. Therefore, when vertical feed lines are present, a more accurate representation for the substrate when scanning in the E-plane is given by

$$Z_{sub}^{E} = \eta\sqrt{\frac{\mu_r}{\epsilon_r}}\frac{d_E}{d_H} \tag{6}$$

$$\beta_{sub}^{E} = k_0\sqrt{\mu_r\epsilon_r}. \tag{7}$$

For H-plane scanning, (4) and (5) remain accurate. The improvement provided by (6)–(7) is illustrated in Fig. 6, where a full wave simulation of the TCDA with an integrated feed is compared to its equivalent circuit using the standard Floquet mode substrate model as well as the proposed TEM substrate model. As seen, the TEM substrate model is significantly more accurate vs. the standard TM Floquet mode substrate model when scanning in the E-plane, especially at lower frequencies. The design details of the feed used in this analysis is discussed in the following sections.

III. Tightly Coupled Dipole Array With an Integrated Balun (TCDA-IB)

Although the above section presents a useful equivalent circuit model for a TCDA radiating element, much of the challenge in developing practical TCDAs lies in the design of the feed circuit itself. The dipoles must be fed differentially, whereas many practical feed networks and electronics employ unbalanced circuits, and a balun is required for each element.

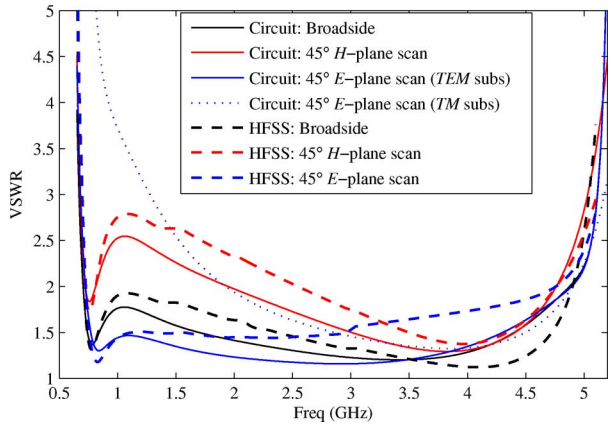

Fig. 6. VSWR of the TCDA with an integrated feed, showing the response of the optimized equivalent circuit from Fig. 8, versus a simulation of the actual array shown in Fig. 9. Note that this model is for a "half" unit cell (as in Fig. 5(b)), without the Wilkinson divider.

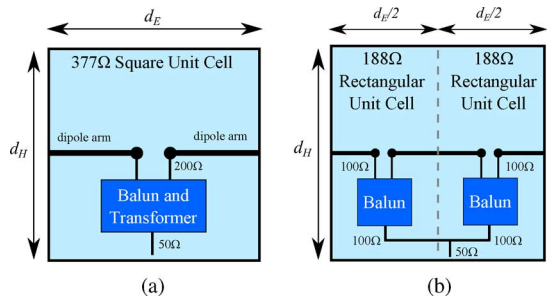

Fig. 7. Top down representation of the unit cell. The impedance of the unit cell is proportional to the aspect ratio d_E/d_H. By splitting the cell into two halves, the impedance of each is correspondingly reduced by a factor of two. Recombining these halves in parallel again reduces the impedance at the common port by another factor of two. (a) Square 377 Ω unit cell. (b) Two 188 Ω "half" unit cells.

Unfortunately, low-loss passive baluns with sufficient bandwidth are often large, heavy, and expensive. Moreover, the input impedance of a TCDA with a square unit cell is typically $\sim$ 200 Ω. Thus, a wideband 50 Ω to 200 Ω transformer is also required, further increasing the size and weight of the feed.

To eliminate the need for the impedance transformer, we may reduce the E-plane dimension d_E of the unit cell by a factor of 2, which correspondingly reduces Z_{TCDA} to $\sim$ 100 Ω. The square unit cell then contains two "half" elements, each comprised of a dipole and a balun (see Fig. 7). However, rather than feeding each half-element individually (which would double the number of phase shifters and T/R modules), the pair can be combined in parallel to provide a single 50 Ω feed. Therefore, the effective element count and unit cell size remains the same, and no impedance transformers are required. A similar "double balun" design uses anti-phase baluns to excite the two arms of a single dipole, realizing a 4:1 impedance bandwidth [11]. The double balun technique has also been shown to significantly reduce cross-polarization by eliminating a common mode resonance which can occur when the combined length of the dipole and feed lines becomes electrically long [9].

Unfortunately, this approach also reduces the available volume since two baluns are required for each element, requiring an extremely compact balun. A Marchand balun,

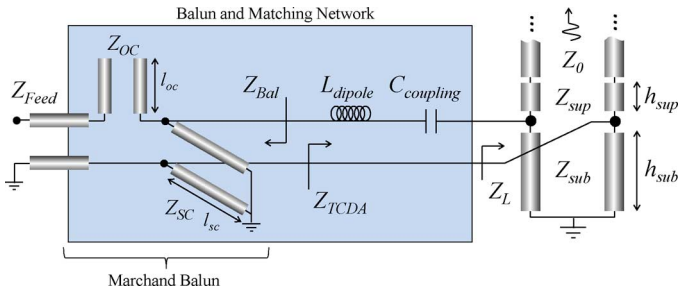

Fig. 8. TCDA-IB equivalent circuit with a Marchand balun feed, adapted from [17]. The addition of the balun's two transmission line stubs increases the overall order of the matching network, leading to increased impedance bandwidth. Optimized circuit values at broadside are: $Z_{Feed} = 100\,\Omega, Z_0 = Z_{sub} = 188\,\Omega$, $Z_{sup} = 144\,\Omega, L_{dipole} = 3.5$ nH, $C_{coupling} = 1.25$ pF, $Z_{OC} = 20\,\Omega$, $Z_{SC} = 169\,\Omega, h_{sub} = 82°, h_{sup} = 59°, l_{oc} = 52°, l_{sc} = 77°$, with all electrical lengths given at 2.5 GHz.

constructed from coupled quarter-wave transmission line stubs (see Fig. 8), is both compact and theoretically capable of operating over a wide bandwidth ($> 10:1$). However, a single stage Marchand balun requires transmission lines with extreme impedance ratios $Z_{OC} \ll Z_{Bal} \ll Z_{SC}$ for wideband operation [16]. With limited available space, implementation of such impedances is challenging. Thus, a standard Marchand balun integrated within a TCDA unit cell will have increased reactance, deteriorating the match and reducing impedance bandwidth. However, if properly tuned, this reactance can be used to compensate for the reactance of the TCDA itself. In this way, together, the balun and TCDA are capable of greater bandwidth than either component provides individually. This technique of matching the reactance of the balun to the reactance of the radiating element is similar to that used in Vivaldi antenna arrays [1].

Referring to the equivalent circuit in Fig. 8, the impedance Z_L, consisting of the substrate, superstrate and radiating transmission lines, is independent of the radiating aperture design and may be thought of as a fixed load to the system. The bandwidth of the TCDA (and all planar arrays) is therefore fundamentally limited by the Fano limit of Z_L, derived in [22], [23]. The standard TCDA of Fig. 2, with series L-C components representing the coupled dipoles, operates as a single stage impedance matching network to Z_L. As shown in Fig. 4, optimization of the circuit model with no feed circuit yielded $\sim 5.5:1$ bandwidth with VSWR $\leq 2:1$ at broadside and VSWR $\leq 2.5:1$ when scanning to 45° in the H-plane. This bandwidth is limited by the simplicity of the single stage impedance match provided by the standard TCDA design. However, if a multi-stage matching network is employed (such as provided by the reactive Marchand balun), this bandwidth can be further increased.

In the circuit of Fig. 8, the stubs Z_{OC} and Z_{SC} along with L_{dipole} and $C_{coupling}$ form a three stage match to Z_L. Through optimization of the circuit, a maximum bandwidth of 8.9:1 (VSWR ≤ 2) was achieved when only broadside scanning was considered. When optimizing over scan using (3)–(7), a 7.3:1 bandwidth was achieved with VSWR ≤ 2 at broadside and VSWR ≤ 2.5 for 45° scanning in all planes. This is a 33% increase in bandwidth from the standard TCDA of Fig. 2. It

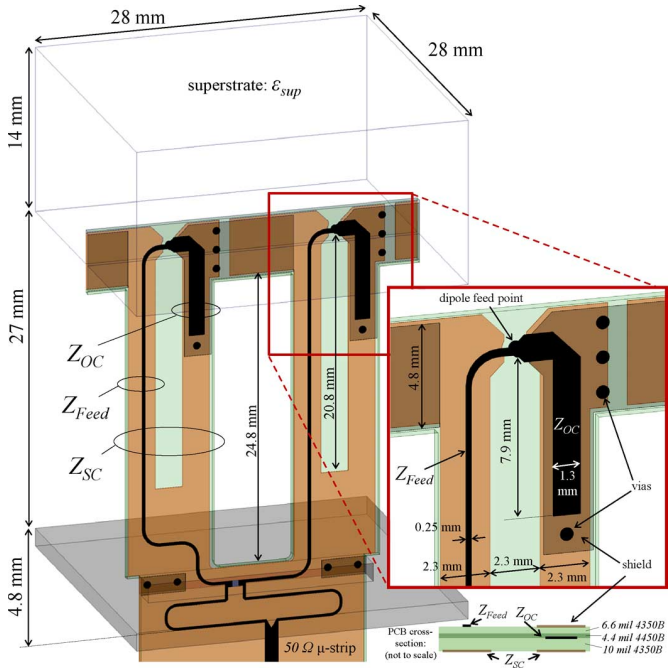

Fig. 9. Implementation of a unit cell of the TCDA-IB. Each unit cell contains two 100 Ω baluns, fed by a single 50 Ω microstrip trace.

also represents a 16% improvement from the design in [17], a result of using the updated scanning circuit model as described above. The performance of the optimized circuit is plotted in Fig. 6.

Therefore, by incorporating the balun within the matching network, the overall bandwidth of the array is increased, while the total size, weight and cost of the array is significantly reduced by eliminating the need for bulky external wideband baluns. We refer to this design as the Tightly Coupled Dipole Array with Integrated Balun (TCDA-IB). We will next discuss the physical implementation of the TCDA-IB.

IV. Physical Implementation of the TCDA-IB

The implementation of the TCDA-IB unit cell is depicted in Fig. 9. The balun and dipole elements are printed together on a 3-layer printed circuit board. The PCB is fabricated from two Rogers 4350B ($\epsilon_r = 3.66$) boards laminated together using a prepreg layer of Rogers 4450B ($\epsilon_r = 3.3$). As before, L_{dipole} is controlled by the width of the dipole arms, which are printed on opposite sides of the board, and $C_{coupling}$ is controlled by the amount of overlap between the arms. We note that Z_{feed} is a 100 Ω microstrip line, and Z_{OC} is implemented in stripline. Z_{SC} is formed by twin vertical metal strips, which also serve as ground planes for Z_{feed} and Z_{OC}. Vias were introduced to connect the upper and lower Z_{OC} grounds and tie the Z_{feed} trace to the Z_{OC} trace at the dipole feed point.

Before attempting to optimize the full unit cell shown in Fig. 9, a rectangular "half" element model (cf. Fig. 5(b)) was developed based on the optimized equivalent circuit. Simple models for the transmission line structures Z_{OC} and Z_{SC} were used to estimate initial dimensions of the balun from the corresponding optimal circuit values, and the design was simulated using Ansys HFSS v.14. By comparing the simulated HFSS

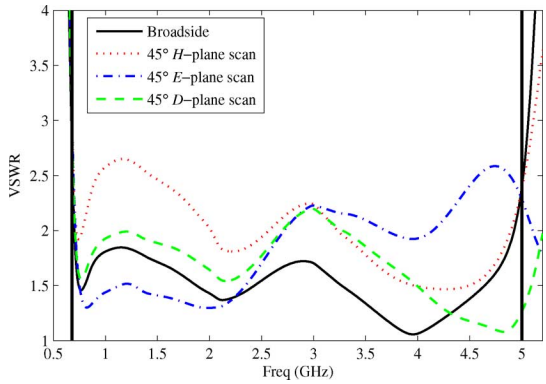

Fig. 10. Simulated VSWR of the TCDA-IB, matched from 0.68–5.0 GHz (7.35:1 BW). This simulation differs from that of Fig. 6 only in that the entire "double" unit cell is modeled with both baluns and the Wilkinson combiner.

response to the circuit model, we could easily identify which components were out of tune, and determine approximate corrections. For this fine-tuning process, it is sufficient for the circuit model to predict the general effect of adjusting a given component, rather than providing an exact match to the physical model. In this manner, the array was fine-tuned quickly and efficiently. Comparison of the optimized equivalent circuit response to the final full-wave simulation (of the "half" unit cell) is shown above in Fig. 6.

Two such "half" elements were then combined to form a full square unit cell (as shown in Fig. 9). The two 100 Ω feeds are combined by a Wilkinson divider below the ground plane to form a single 50 Ω microstrip trace. The simulated VSWR for the complete "double" unit cell, computed at the common 50 Ω input is given in Fig. 10. The array achieves 7.35:1 impedance bandwidth (0.68–5.0 GHz) with $\mathrm{VSWR} \leq 2$ at broadside, and $\mathrm{VSWR} \leq 2.65$ when scanning to 45° in all planes. The realized gain and radiation efficiency of the array as seen in Fig. 11 a is high, with total ohmic and mismatch losses < 0.5 dB at broadside and < 1.3 dB over the scan volume. The cross-polarization (using Ludwig's third definition [24]) is also low, except in the D-plane at the top of the band, where it exceeds -10 dB. However, this cross polarization is reduced when a second orthogonal polarization is added, as we show below in Section V.

The width of all printed lines and spaces is ≥ 0.13 mm (10 mil) and the entire structure can be easily manufactured using standard low-cost printed circuit board technology. The design may be scaled to operate at frequencies up to ~ 10 GHz. However, when scaling to higher frequencies, reoptimization to accommodate manufacturing tolerances may result in reduced bandwidth. Nevertheless, the smallest features (e.g., width of the feed trace, PCB thickness, via size, etc.) are not resonant dimensions and would not necessarily need to be directly scaled.

If desired, T/R modules or phase shifters can be integrated directly on the circuit board below the ground plane, after the Wilkinson divider, resulting in a low cost compact electronically scanning array. This level of integration is not possible with a standard TCDA, because of the need for external baluns located between the array and electronics.

The above design represents an improvement in bandwidth as compared to the preliminary design in [17]. The updated

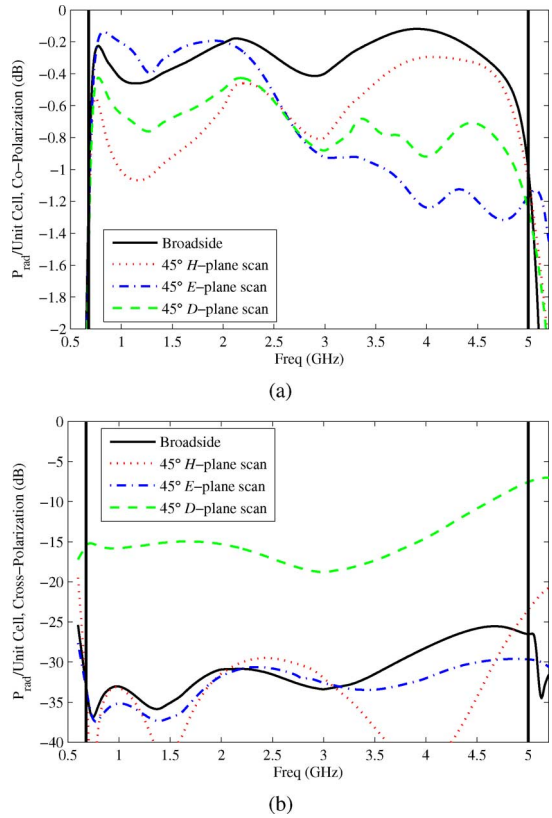

Fig. 11. Simulated gain per unit cell of the TCDA-IB (a) Co-Polarization. (b) Cross-Polarization using Ludwig's third definition. (a) Co-Polarized Gain. (b) Cross-Polarized Gain.

array uses higher impedances for the balun's transmission line stubs, a significantly longer open-circuited stub, and minor adjustments to the other dimensions. However, the primary difference is that the improved circuit model enables more effective optimization and tuning of the array. As an example, optimization of the previous circuit model provides an initial superstrate thickness of 22 mm [17]. This circuit was optimized for broadside and H-plane scanning, but not for E-plane scanning due to poor accuracy, as described above. Full-wave simulations of this configuration revealed large mismatches when scanning in the E-plane, and the superstrate had to then be manually reduced to 12.7 mm. Such manual adjustments require numerous lengthy simulations, and obtaining an optimal design is challenging. By contrast, the improved circuit model in Fig. 8 using (3)–(7) can be simultaneously optimized for broadside, H-plane, and E-plane scanning, yielding an initial superstrate thickness of 15 mm. Subsequent fine-tuning of the design resulted in only a minor adjustment of the superstrate to 14 mm. Thus, the updated circuit model enables more efficient optimization over the array over the entire scan volume, and produces a design with superior performance.

A. Avoiding Undesired Resonances Within the TCDA-IB

There are several practical issues that must also be considered when designing the TCDA-IB to avoid undesired modes and detrimental resonances. The problem of common mode currents is well known for tightly coupled and connected arrays.

These common modes were described in [14] and [25], and correspond to a resonance between adjacent vertical feeds. For the TCDA-IB, this mode forms when d_H (the distance between the feed boards) reaches a half-wavelength. However, excessive reduction of d_H results in oversampling and increased T/R module costs. For our design, the element spacing in both dimensions is set at 28 mm, which is 93% of $\lambda/2$ at 5 GHz.

Another undesired resonance can occur within the balun if there is direct parasitic coupling between the open circuited stub Z_{OC} and the trace Z_{feed}. We avoid this resonance by extending one of the dipole arms as a shield for the Z_{OC} stub, converting it from a microstrip to a stripline (see Fig. 9). This also helps to lower the impedance Z_{OC}, further improving the balun's bandwidth.

Surface waves present another possible source of resonances in scanning arrays. These occur when the array structure supports a traveling wave at a particular scan angle. For TCDAs, surface waves may potentially form in either the superstrate or the substrate layers, if high contrast materials are used. Here, we avoid surface waves by using a superstrate having a relatively low dielectric constant of $\epsilon_{sup} = 1.7$, and an air substrate.

When connecting the two baluns together to form a single feed for the double element, it might be assumed that a reactive split would be desirable to minimize resistive losses. However, this allows a loop resonance to form between the two elements when the array is scanned. Such a resonance is prevented by using a matched Wilkinson divider, which provides isolation between the two balun circuits. Unlike the standard Wilkinson design with three 50 Ω ports, this design has a single 50 Ω input and two 100 Ω outputs, resulting in a frequency independent impedance match. The isolation between the output ports does depend on the electrical length of the divider and is therefore band limited. However, it is not necessary to maintain perfect isolation in order to suppress the loop resonance, and a single stage divider was found to be sufficient. We note that unlike the claims in [26], we did not observe unacceptable losses when scanning in the E-plane. As seen in Fig. 11(a), the worst-case loss is 1.3 dB at the top of the band, which represents ~ 0.5 dB reactive loss due to impedance mismatch and ~ 0.8 dB ohmic losses. To minimize the space required below the ground plane, the Wilkinson is meandered as shown in Fig. 9.

The vertical PCB is installed in the ground plane through a slot which is sufficiently wide to allow the microstrip feed and Wilkinson to pass through. However, if the slot is too long it may resonate due to the dielectric loading from the PCB. Therefore, vias are introduced at the edges of the PCB card in the slot to reduce its electrical width to under $\lambda/2$ in the dielectric, as shown in Fig. 9. Electrical connection between the PCB ground and the array ground plane is maintained along the back of the slot using conducting gasket or fingerstock. Additional construction details, as well as measured results from an earlier TCDA-IB design are provided below in Section VI.

V. A Dual-Polarized TCDA-IB

Many wideband array applications require dual-linear or dual-circular polarizations. Therefore, it may be desired to add a second orthogonal set of elements to the TCDA-IB array. For arrays printed on vertical printed circuit boards, a common manner of constructing a dual-polarized array is to use an "egg-crate" construction, in which partial slots are cut to allow crossing boards to fit together as shown in Fig. 12. To minimize interference between baluns, the boards do not cross at the feed centers, but rather cross at the overlapping capacitive sections yielding elements with offset phase centers, similar to [14].

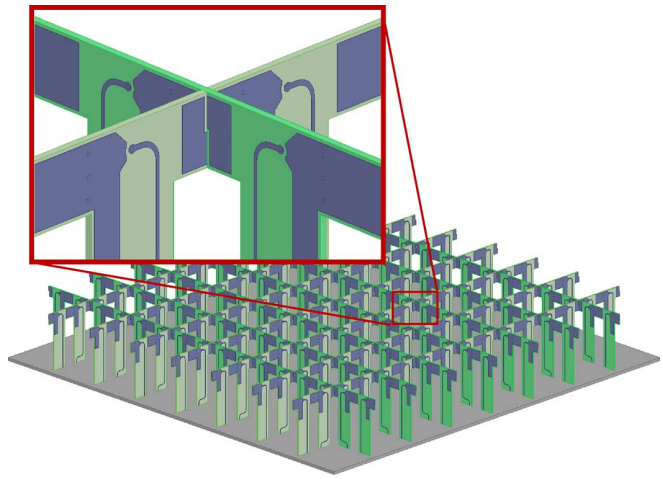

Fig. 12. "Egg-crate" implementation of dual-polarized TCDA-IB. Orthogonal elements intersect at the coupling capacitance via a partial slot cut in both boards. The elements are otherwise unchanged from the single-polarized design of Fig. 9. A small gap is preserved between the orthogonal elements and no soldering is required at the joint.

No direct electrical connection or soldering is required at the joints, allowing for simple assembly and maintenance of the dual-polarized array. A small 0.010" gap is maintained between the metallization of the orthogonal elements, which can be controlled by inserting a dielectric shim or tape between the boards, or by adding unmetallized outer layers to the PCB. Parametric analysis indicates that the gap may be varied from 0.005–0.015" without significant impact on the performance of the array. Other than the addition of the slot and a minor compensation of the dipole capacitance, the dual-polarized element is unchanged from the single-polarized design above.

The simulated VSWR, co-polarized gain, and cross-polarized gain of the dual polarized TCDA-IB unit cell are shown in Fig. 13. Other than a slight reduction in impedance bandwidth to 6.9:1 (which may be improved by additional fine tuning of the dual-polarized design), the VSWR and co-polarized gain are similar to the single polarized TCDA-IB (cf. Figs. 10–11(a)). However, the addition of the second polarization reduced the cross-polarization by $\sim$ 5 dB from the single polarized design (cf. Fig. 11(b)). Specifically, the cross polarization is now < -20 dB over the majority of the band, with a worst case of -13 dB in the 45° D-plane at the top of the band. The port-to-port coupling between the orthogonal elements is shown in Fig. 14 and is < -30 dB at broadside and < -15 dB when scanning in the D-plane.

VI. Prototype TCDA-IB Design Construction and Measured Results

An 8×8 prototype TCDA-IB was constructed, as pictured in Fig. 15. The prototype array is based on the TCDA-IB design given in [17], which has a slightly lower simulated band-

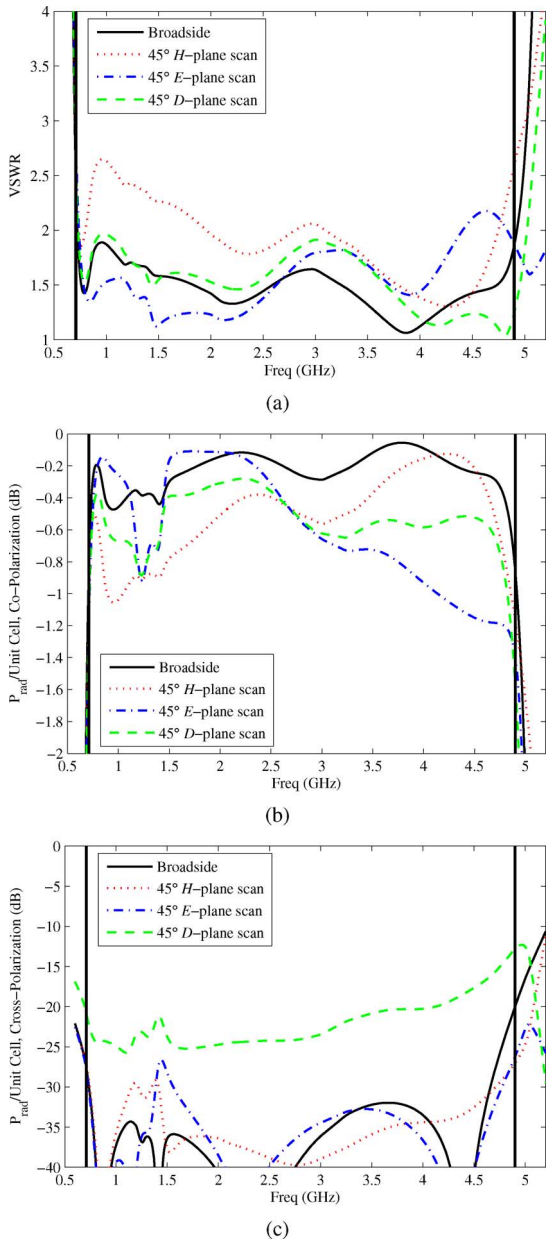

Fig. 13. Simulated VSWR and gain of the dual-polarized TCDA-IB, with one polarization excited and the other terminated. (a) VSWR, matched to $< 2.65:1$ in all scan planes from 0.71–4.9 GHz (b) Co-Polarized Gain (b) Cross-Polarized Gain using Ludwig's third definition. (a) Dual-Polarized TCDA-IB, VSWR. (b) Dual-Polarized TCDA-IB, Co-Polarized Gain. (c) Dual-Polarized TCDA-IB, Cross-Polarized Gain.

width of 6.3:1 (0.69–4.37 GHz). The design is similar to that presented above in Section IV, but was designed prior to the development of the improved TCDA scanning circuit model described in Section II-B. Thus, it is not optimized as efficiently as the improved TCDA-IB design of Fig. 9.

To terminate the edges of the array, the dipole arms were extended by an additional 60 mm, effectively adding 2 rows of short-circuited elements. Terminating the array in this manner was suggested in [27] as a method to improve gain bandwidth without reducing efficiency, which can suffer when using resistively terminated edge elements.

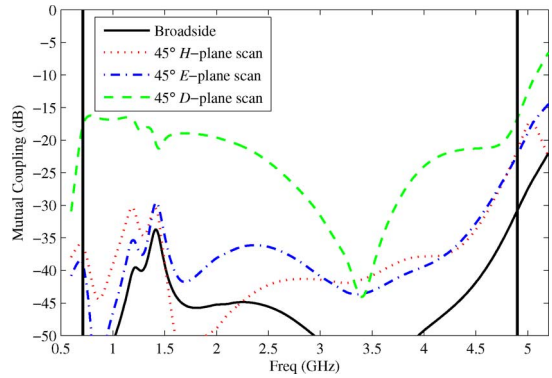

Fig. 14. Simulated coupling between the neighboring orthogonal elements within the dual-polarized TCDA-IB array of Fig. 12.

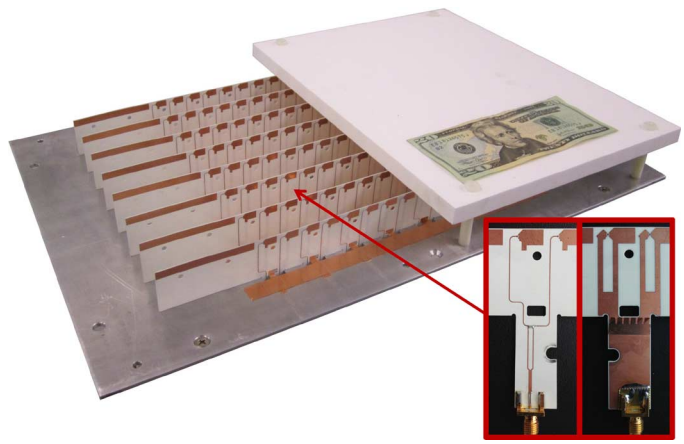

Fig. 15. Photograph of the fabricated 8×8 TCDA-IB prototype from [17] with half of the superstrate removed to show the array details. Note the extended dipole arms of the edge elements. Inset shows a closeup of the front and back sides of a single element printed on PCB card.

The array was constructed on a 12"$\times$ 18" aluminum plate and was covered by a 12.7 mm (0.5") thick superstrate ($\epsilon_{sup} = 1.7$) of the same size, held in place by small nylon rods around the perimeter of the array. The height of the array is 45 mm (1.77") from the top of the superstrate to the ground plane, and 63.5 mm (2.5") to bottom of the Wilkinson. The active area of the 64 elements is 576 cm^2 (89 in^2). When the extended dipole arms are included, the total area of the array is 864 cm^2 (134 in^2). Rectangular holes were cut in the ground plane allowing the vertical cards to be installed, which were held in place by right angle brackets below the ground plane. If additional mechanical support is required, rigid foam blocks may be used to reinforce the vertical cards and superstrate. This should not affect the desired performance of the array. A 50 Ω SMA connector was installed on each element, which is in turn fed by a matched 64:1 divider located below the ground plane. The array was scanned by adjusting the lengths of the feed cables.

Conductive tape was used to reduce the size of opening in the ground plane after the elements were installed. Note that this is unnecessary for TCDA-IB design presented in Section III, due to the introduction of grounding vias in the PCB. The prototype array also uses a longer, straight Wilkinson divider rather than the compact design shown in Fig. 9.

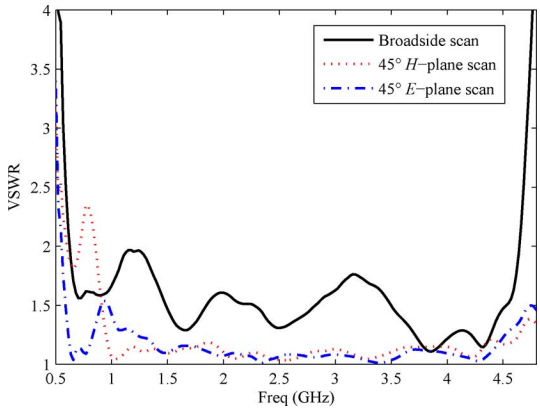

Fig. 16. Measured VSWR of the TCDA-IB prototype from [17], measured through a 64:1 matched power divider. The return loss was compensated for the round trip insertion loss of the power divider and cables. Scanning VSWR is artificially low due to out-of-phase reflections absorbed within the power divider.

The measured VSWR of the array is shown in Fig. 16 and is less than 2:1 at broadside and under 2.5:1 while scanning to $\pm 45^\circ$ in both planes over the entire operational band (0.67–4.37 GHz). The measurement was taken at the common port of the 64:1 divider, and the VSWR data has been compensated by the round trip insertion loss of the divider and cables. Note that when scanning, the reflections from the elements are not in-phase and thus the reflected power is mostly absorbed within the power divider, resulting in artificially low measured VSWR at the common port.

The array was then mounted to a larger 4' $\times$ 6' ground plane and measured in The Ohio State University's anechoic chamber. The measured gain of the array is shown in Figs. 17–20 at broadside and when scanning to 45° in the E-, H-, and D-planes. Again, the gain has been offset by the measured insertion loss of the power divider and cables. The simulated gain of the finite array is also plotted, along with the theoretical gain limit for the aperture area. This limit is computed using both the area of only the actively fed elements, as well as the total area including the extended dipoles. Because the extended dipoles increase the effective aperture size in the E-plane dimension, the H-plane beam is slightly broader than the E-plane beam, especially at lower frequencies, as seen in Fig. 17(b). Some beam broadening and beam squint is also apparent between 2–3 GHz, which is thought to be due to edge-launched waves that occur in finite tightly coupled and connected arrays [8], [28]. Because such waves propagate along the dipoles, the effects are seen more strongly in the E-plane than in the H-plane. However, the gain is within 3 dB of the theoretical limit in all scan-planes over a 6.6:1 bandwidth (0.67–4.37 GHz), and the measured performance matches the simulations very well. Furthermore, the cross-polarized gain (using Ludwig's third definition) of the array is more than 15 dB below that of the co-polarized gain over the majority of the band, though it exceeds -10 dB in the D-plane at the top end of the band. As noted above, the cross-polarization can be significantly mitigated in a dual-polarized implementation.

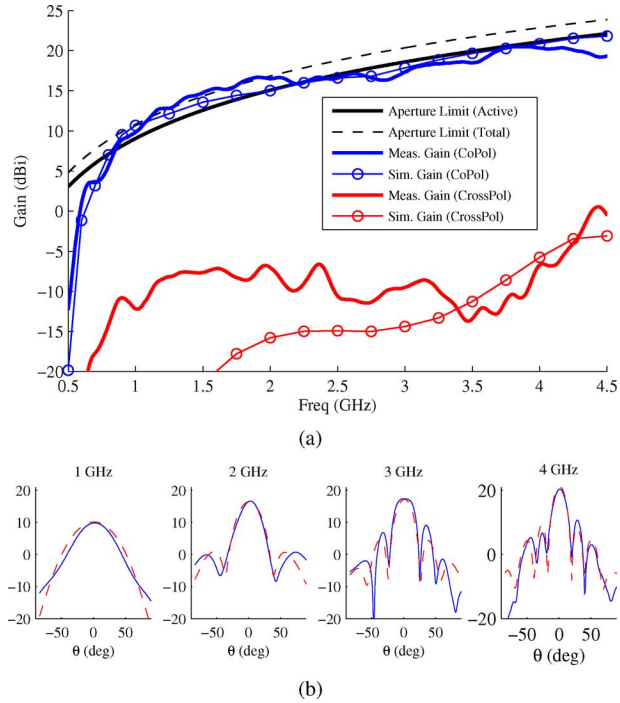

Fig. 17. Measured co- and cross-polarized gain of the 8 $\times$ 8 TCDA-IB prototype from [17] at broadside. (a) Gain at broadside vs. frequency. Also plotted is the theoretical aperture limit for the array, calculated using the area of the active elements, as well as the total area including the extended dipole arms. (b) Measured patterns in E-plane (blue solid) and H-plane (red dotted) at several frequencies.

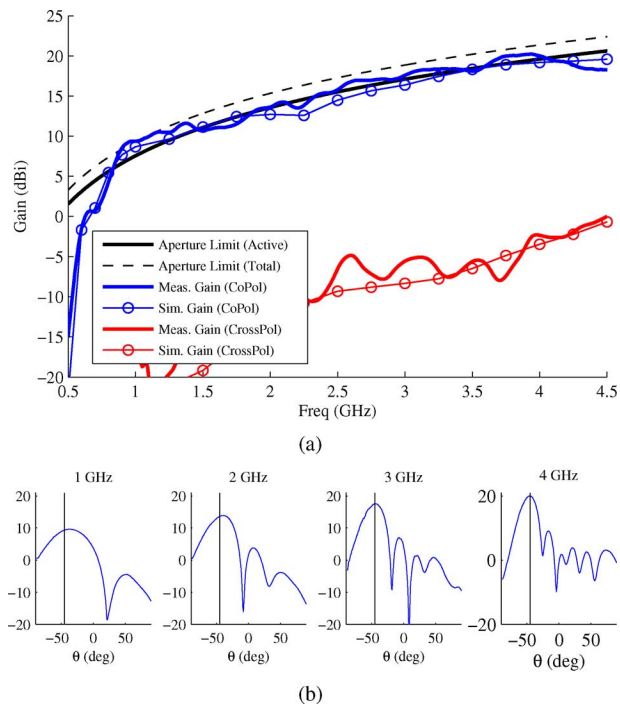

Fig. 18. Measured gain of the TCDA-IB prototype from [17], scanning to 45° in the H-Plane. (a) Gain vs. frequency at nominal beam center. (b) Gain pattern in H-plane at several frequencies. The nominal beam center at 45° is noted by a vertical line.

VII. Conclusions

A new technique for feeding TCDAs has been developed, to significantly improve the impedance bandwidth and scanning

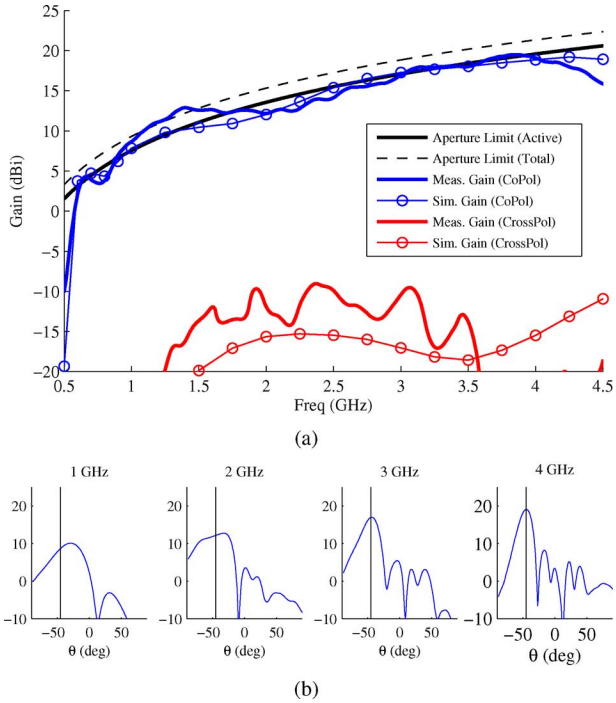

Fig. 19. Measured gain of the TCDA-IB prototype from [17], scanning to 45° in the E-Plane. (a) Gain vs. frequency at nominal beam center. (b) Gain pattern in E-plane at several frequencies. The nominal beam center at 45° is noted by a vertical line.

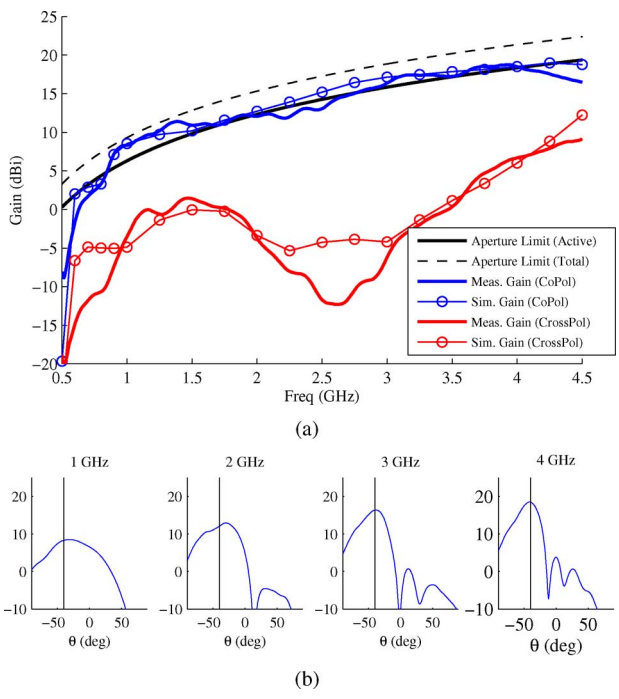

Fig. 20. Measured gain of the TCDA-IB prototype from [17], scanning to 45° in the D-Plane. (a) Gain vs. frequency at nominal beam center. (b) Gain pattern in D-plane at several frequencies. The nominal beam center at 45° is noted by a vertical line. For D-plane scanning only 48 of 64 elements were excited, with 16 elements (located in two corners of the array) terminated.

performance of the array, while enabling a dramatic reduction in overall size, weight and cost. We show that a simple Marchand balun can also be used as a multi-stage impedance matching network for the array, resulting in a bandwidth improvement of over 30% as compared to a standard TCDA. Our TCDA-IB design has a total height of only $0.76\lambda_{high}$ ($0.68\lambda_{high}$ above the ground plane), and achieves an impedance bandwidth of 7.35:1 with a low VSWR of $< 2.65 : 1$ over the entire $\pm 45°$ scan volume. The baluns are printed on the same substrate as the array itself, and thus their cost and weight is minimal. Further, T/R modules or phase shifters can be integrated directly onto the same PCB below the ground plane, enabling an extremely compact wideband electronically scanned array.

An 8×8 element prototype array was built to validate the approach, based on a preliminary design described in [17] with a slightly lower simulated bandwidth of 6.3:1. Short circuited elements (i.e., extended dipoles) were used to terminate the edges of the array and mitigate edge effects; thus lossy terminations that could reduce efficiency were avoided. The prototype performed very well relative to simulation with a measured operational bandwidth of 6.6:1 while scanning to $\pm 45°$ in all directions.

Our TCDA-IB is a simple, low cost array system with extremely wide bandwidth and excellent scanning capabilities. We believe that the TCDA-IB is the first low-profile array capable of greater than 7:1 bandwidth while maintaining a low impedance mismatch ($\mathrm{VSWR} < 2.65 : 1$) over a large scan volume ($\pm 45°$), and which does not require active or external baluns, or lossy materials. Therefore, the TCDA-IB is an attractive technology for a variety of wideband communication and sensing applications, and for small and low-cost platforms.

REFERENCES

[1] J. Shin and D. H. Schaubert, "A parameter study of stripline-fed Vivaldi notch-antenna arrays," *IEEE Trans. Antennas Propag.*, vol. 47, no. 5, pp. 879–886, May 1999.

[2] M. W. Elsallal and J. C. Mather, "An ultra-thin, decade (10:1) bandwidth, modular BAVA array with low cross-polarization," in *Proc. IEEE Antennas Propag. Soc. Int. Symp. (APSURSI)*, Jul. 2011, pp. 1980–1983.

[3] J. G. Maloney, B. N. Baker, R. T. Lee, G. N. Kiesel, and J. J. Acree, "Wide scan, integrated printed circuit board, fragmented aperture array antennas," in *Proc. IEEE Antennas Propag. Soc. Int. Symp. (APSURSI)*, Jul. 2011, pp. 1965–1968.

[4] W. F. Moulder, K. Sertel, and J. L. Volakis, "Superstrate-enhanced ultrawideband tightly coupled array with resistive FSS," *IEEE Trans. Antennas Propag.*, vol. 60, no. 9, pp. 4166–4172, 2012.

[5] B. A. Munk, "Broadband wire arrays," in *Finite Antenna Arrays and FSS*, 1st ed. Hoboken, NJ, USA: Wiley-IEEE Press, 2003, ch. 6, pp. 181–213.

[6] B. Munk *et al.*, "A low-profile broadband phased array antenna," in *Proc. IEEE Antennas Propag. Soc. Int. Symp. (APSURSI)*, Jun. 2003, vol. 2, pp. 448–451.

[7] J. L. Volakis and K. Sertel, "Narrowband and wideband metamaterial antennas based on degenerate band edge and magnetic photonic crystals," *Proc. IEEE*, vol. 99, no. 10, pp. 1732–1745, Oct. 2011.

[8] J. A. Kasemodel, C.-C. Chen, and J. L. Volakis, "Wideband planar array with integrated feed and matching network for wide-angle scanning," *IEEE Trans. Antennas Propag.*, 2013, to be published.

[9] D. Cavallo, A. Neto, and G. Gerini, "PCB slot based transformers to avoid common-mode resonances in connected arrays of dipoles," *IEEE Trans. Antennas Propag.*, vol. 58, no. 8, pp. 2767–2771, Aug. 2010.

[10] D. Cavallo, A. Neto, and G. Gerini, "A wideband (3 to 5 GHz) wide-scan connected array of dipoles with low cross polarization," in *Proc. EuCAP – Eur. Conf. on Antennas Propag.*, Mar. 2012, pp. 3239–3242.

[11] W. R. Pickles, "Double Balun Dipole," U.S. Patent US8350774 B2, Jan. 2013.

[12] R. L. Li, T. Wu, B. Pan, K. Lim, J. Laskar, and M. M. Tentzeris, "Equivalent-circuit analysis of a broadband printed dipole with adjusted integrated balun and an array for base station applications," *IEEE Trans. Antennas Propag.*, vol. 57, no. 7, pp. 2180–2184, Jul. 2009.

[13] P. Lindberg, E. Öjefors, Z. Barna, A. Thornell-Pers, and A. Rydberg, "Dual wideband printed dipole antenna with integrated balun," *IET Microw., Antennas Propag.*, vol. 1, no. 3, p. 707, 2007.
[14] S. S. Holland and M. N. Vouvakis, "The planar ultrawideband modular antenna (PUMA) array," *IEEE Trans. Antennas Propag.*, vol. 60, no. 1, pp. 130–140, Jan. 2012.
[15] C. A. Balanis, Ed., Modern Antenna Handbook1st ed. Hoboken, NJ, USA, Wiley-Interscience, 2008.
[16] D. M. L. Bartholomew, "Optimum design for a broadband microstrip balun," *Electron. Lett.*, vol. 13, no. 17, pp. 510–511, Aug. 1977.
[17] J. P. Doane, K. Sertel, and J. L. Volakis, "A 6.3:1 bandwidth scanning tightly coupled dipole array with co-designed compact balun," in *Proc. IEEE Antennas Propag. Soc. Int. Symp. (APSURSI)*, Jul. 2012, pp. 1–2.
[18] J. P. Doane, K. Sertel, and J. L. Volakis, "A wideband scanning conformal array with a compact compensating balun," in *Proc. Antennas Applicat. Symp.*, Allerton, IL, Sep. 2012, pp. 58–69.
[19] A. K. Bhattacharyya, "Floquet modal functions," in *Phased Array Antennas : Floquet Analysis, Synthesis, BFNs and Active Array Systems*, 1st ed. Hoboken, NJ, USA: Wiley-Interscience, 2006, ch. 3.
[20] H. A. Wheeler, "The radiation resistance of an antenna in an infinite array or waveguide," *Proc. IRE*, vol. 36, no. 4, pp. 478–487, Apr. 1948.
[21] D. Cavallo, A. Neto, and G. Gerini, "Analytical description and design of printed dipole arrays for wideband wide-scan applications," *IEEE Trans. Antennas Propag.*, vol. 60, no. 12, p. 1, Dec. 2012.
[22] J. P. Doane, K. Sertel, and J. L. Volakis, "Analytical description and design of printed dipole arrays for wideband wide-scan applications," *Electron. Lett.*, vol. 48, no. 10, p. 540+, 2012.
[23] J. P. Doane, K. Sertel, and J. L. Volakis, "Matching bandwidth limits for arrays backed by a conducting ground plane," *IEEE Trans. Antennas Propag.*, vol. 61, no. 5, pp. 2511–2518, May 2013.
[24] A. Ludwig, "The definition of cross polarization," *IEEE Trans. Antennas Propag.*, vol. 21, no. 1, pp. 116–119, Jan. 1973.
[25] S. S. Holland and M. N. Vouvakis, "The banyan tree antenna array," *IEEE Trans. Antennas Propag.*, vol. 59, no. 11, pp. 4060–4070, Nov. 2011.
[26] D. Cavallo, "Connected Array Antennas: Analysis and Design," Ph.D. dissertation, Technische Universiteit Eindhoven, The Netherlands, 2011.
[27] I. Tzanidis, K. Sertel, and J. L. Volakis, "Characteristic excitation taper for ultrawideband tightly coupled antenna arrays," *IEEE Trans. Antennas Propag.*, vol. 60, no. 4, pp. 1777–1784, Apr. 2012.
[28] A. Neto, D. Cavallo, and G. Gerini, "Edge-born waves in connected arrays: A finite infinite analytical representation," *IEEE Trans. Antennas Propag.*, vol. 59, no. 10, pp. 3646–3657, Oct. 2011.

Jonathan Doane (M'13) received the B.Sc. and M.Sc. degrees from Michigan Technological University, Houghton, MI, USA, in 1999 and 2001, respectively, and the Ph.D. degree from the Ohio State University, Columbus, OH, USA, in 2013.

Prior to returning to grad school in 2010, he worked at Rockwell Collins' Advanced Technology Center on electrically small and multifunction antennas. He recently joined the RF and Quantum Systems Technology group at MIT Lincoln Laboratories. His research interests include wideband and low-profile antenna arrays.

Dr. Doane received the Best Student Paper Award at the 2012 IEEE Antennas and Propagation Symposium.

Kubilay Sertel (SM'07) received the Ph.D. degree in 2003 from the Electrical Engineering and Computer Science Department at the University of Michigan-Ann Arbor, MI, USA.

He is currently an Assistant Professor at the Electrical and Computer Engineering Department at the Ohio State University, Columbus, OH, USA. He was a Research Scientist at the ElectroScience Laboratory and an Adjunct Professor at the Electrical and Computer Engineering Department at the Ohio State University during 2003–2012. His current research focuses on the analysis and design of THz and mmW sensors, antennas arrays and spectroscopy systems for biomedical and non-destructive imaging, as well as ultra wideband low-profile antennas and phased arrays for cognitive sensing and opportunistic wireless networks, reconfigurable antennas, arrays and miniaturization techniques, novel RF materials, frequency selective surfaces/volumes and magneto-dielectric metamaterials, measurement and characterization of anisotropic composites. His expertise also includes applied electromagnetic theory and computational electromagnetics, particularly, curvilinear fast multipole modeling of hybrid integral equation/finite element systems and efficient solution of large-scale, real-life problems on massively parallel supercomputing platforms. He coauthored two books, *Frequency Domain Hybrid Finite Element Methods in Electromagnetics* (Morgan & Claypool, 2006), *and Integral Equation Methods for Electromagnetics* (SciTech Publishing, 2012), and published over 50 journal papers and over 170 conference articles.

Prof. Sertel is an elected member of URSI Commission B, and a member of Applied Computational Electromagnetics Society.

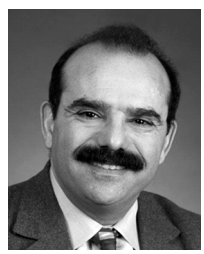

John L. Volakis (S'77–M'82–SM'89–F'96) was born on May 13, 1956 in Chios, Greece and immigrated to the U.S. in 1973. He received the B.E. degree (*summa cum laude)* in 1978 from Youngstown State University, Youngstown, OH, USA, the M.Sc. and Ph.D. degrees from The Ohio State University, Columbus, OH, USA, in 1979 and 1982, respectively.

He started his career at Rockwell International (1982–1984), now Boeing. In 1984, he was appointed Assistant Professor at The University of Michigan, Ann Arbor, MI, USA, becoming a Full Professor in 1994. He also served as the Director of the Radiation Laboratory from 1998 to 2000. Since January 2003, he is the Roy and Lois Chope Chair Professor of Engineering at The Ohio State University, Columbus, and also serves as the Director of the ElectroScience Laboratory. Over the years, he carried out research in antennas, wireless communications and propagation, computational methods, electromagnetic compatibility and interference, design optimization, RF materials, multi-physics engineering, bioelectromagnetics, terahertz, and medical sensing. His publications include eight books (among them: *Approximate Boundary Conditions in Electromagnetics* (IEEE Press, 1995); *Finite Element Methods for Electromagnetics* (IEEE Press, 1998); *4th edition Antenna Engineering Handbook* (McGraw Hill, 2007); *Small Antennas* (McGraw Hill, 2010); and *Integral Equation Methods for Electromagnetics* (Scitech Publishing, 2012). He has also published over 320 journal papers, nearly 600 conference papers and 23 book chapters.

Prof. Volakis has graduated/mentored over 70 doctoral students/post-docs with 20 of them receiving best paper awards at conferences. His service to professional societies include: 2004 President of the IEEE Antennas and Propagation Society, twice the General Chair of the IEEE Antennas and Propagation Symposium, IEEE APS Distinguished Lecturer, IEEE APS Fellows Committee Chair, IEEE-wide Fellows committee member and Associate Editor of several journals. He is listed by ISI among the top 250 most referenced authors (2004), and is a Fellow of IEEE and ACES. Among his awards are: The Univ. of Michigan College of Engineering Research Excellence award (1993), Scott award from The Ohio State Univ. College of Engineering for Outstanding Academic Achievement (2011) and the IEEE AP Society C-T. Tai Teaching Excellence award (2011).